Effective elastic mechanical properties of single layer graphene sheets

F Scarpa[1,4], S Adhikari[2] and A Srikantha Phani[3]

[1] Department of Aerospace Engineering, University of Bristol, Bristol BS8 1TR, UK
[2] School of Engineering, University of Wales Swansea, UK
[3] Department of Mechanical Engineering, The University of British Columbia, Vancouver, Canada

E-mail: f.scarpa@bris.ac.uk and scarpa.fabrizio@gmail.com

Abstract
The elastic moduli of single layer graphene sheet (SLGS) have been a subject of intensive research in recent years. Calculations of these effective properties range from molecular dynamic simulations to use of structural mechanical models. On the basis of mathematical models and calculation methods, several different results have been obtained and these are available in the literature. Existing mechanical models employ Euler–Bernoulli beams rigidly jointed to the lattice atoms. In this paper we propose truss-type analytical models and an approach based on cellular material mechanics theory to describe the in-plane linear elastic properties of the single layer graphene sheets. In the cellular material model, the C–C bonds are represented by equivalent mechanical beams having full stretching, hinging, bending and deep shear beam deformation mechanisms. Closed form expressions for Young's modulus, the shear modulus and Poisson's ratio for the graphene sheets are derived in terms of the equivalent mechanical C–C bond properties. The models presented provide not only quantitative information about the mechanical properties of SLGS, but also insight into the equivalent mechanical deformation mechanisms when the SLGS undergoes small strain uniaxial and pure shear loading. The analytical and numerical results from finite element simulations show good agreement with existing numerical values in the open literature. A peculiar marked auxetic behaviour for the C–C bonds is identified for single graphene sheets under pure shear loading.

(Some figures in this article are in colour only in the electronic version)

1. Introduction

Graphene sheets (GS) have Young's modulus and thermal conductivity rivalling that of graphite (1.06 TPa and 3000 W m^{-1} K^{-1} respectively) [1, 2]. They may exist as single layered or multi-layer structures. It is possible to harness the multifunctional properties of graphene sheets and design novel class of advanced composites with superior mechanical and electric performance [1–3], as well as innovative strain sensors [5]. An approach to produce graphene–polymer composites by complete exfoliation of graphite and molecular-level dispersion of GS in a polymer host has been described in [4]. The latter work, from Stankovich *et al*, has fuelled

a growing interest into the mechanical determination and characterization of single layer graphene sheets (SLGS), although from the experimental point of view advances have been made in measuring magneto-transport properties [9], while experimental mechanical data are still confined to graphene layers only. The enhanced flexibility of GS, despite their high Young's modulus, has been attributed to the change in curvature given by reversible elongation of sp^2 C–C bonds [6, 8, 49]. Vibrational properties of SLGS [10] or multi-layer graphene assemblies [7] have also been evaluated using analytical and finite element simulation methods.

Molecular mechanistic modelling of single layer graphene sheets has been pursued by several authors. Simple lattice models with force constants derived from an assumed potential have been developed by Bacon and Nicholson [11] and Gillis [12]. *Ab initio* methods have been used by

---

Kudin *et al* [13], who predict a Young's modulus of 1.02 TPa and Poisson's ratio of 0.149, and Van Lier *et al* [14], reporting a Young's modulus for graphene equal to 1.11 TPa. Several authors have made use of Tersoff–Brenner potentials to describe the mechanical properties of single graphene sheets, with Young's modulus predictions between 0.694 and 0.714 TPa, and Poisson's ratios from 0.397 to 0.417 [15, 16]. Brenner's potential and Cauchy–Born rule have also been used by Reddy *et al* [23] to describe the mechanical properties of finite size graphene sheets, highlighting the difference between minimized and unminimized strain energy configurations for the SLGS under different types of loading. Rajendran and Reddy have also indicated the maximum numerical precision attainable using the above methods to calculate the stiffness of SLGS and carbon nanotubes [22]. Second generation Brenner potentials have also been used by Huang *et al* [17] to calculate the in-plane Young's moduli, Poisson's ratios and thickness of GS and single wall carbon nanotubes (SWCNTs), with stiffness values for the GS ranging from 2.99 to 4.23 TPa, and Poisson's ratio of around 0.397. A rigorous homogenization technique has been also developed by Caillerie *et al* [25] to calculate first Piola–Kirchhoff and Cauchy stress tensors considering stretching and bond angle variation. Other analytical models of SLGS incorporating energy contributions from bond stretching and changes in bond angle have been proposed as subset of analogous models for single wall carbon nanotubes, [50]. The mechanical properties of different graphene configurations, with chiral index n towards infinity, have been extracted from analytical nanotubes models. Hemmasizadeh *et al* [24] have also used a mixed MD–continuum mechanics model based on thin shell theory to obtain the properties of SLGS from a numerical nanoindentation simulation.

Another approach widely used recently for nanostructures modelling is the equivalent atomistic continuum–structural mechanics approach, pioneered by Odegard *et al* [18] and Li and Chou [19]. In this approach, typical elements of structural mechanics, such as rods, beams and shells are used with appropriate mechanical properties to simulate the static and dynamic behaviour of graphene layers and carbon nanotubes. The mechanical properties for the structural elements are derived from equilibrium between harmonic steric potentials of the C–C bonds and mechanical strain energies associated to tension, torsion and bending related to the mechanical elements simulating the bonds themselves. A truss model was proposed in [18], wherein rods of different stiffnesses represent the stretching and in-plane bending capabilities of the C–C bonds. Reddy *et al* [21] extended the model from [18] to account for the orthotropy generated in finite size graphene sheets. Meo and Rossi [20] developed a finite element model comprising uniaxial links and nonlinear rotational spring to represent the modified Morse potential when simulating graphene and carbon nanotube structures. Tserpes and Papanikos [33] identified thickness and stiffness properties (Young's and shear modulus) for an equivalent material associated to the C–C bonds represented by finite element beams in single walled carbon nanotubes (SWCNTs). The approach of [33] has been used by Sakhaee-Pour *et al* [10] to compute natural frequencies

and modes of single graphene sheets, and to characterize the in-plane properties of SLGS with different chirality [34].

The wide dispersion of the mechanical properties of graphene sheets can be attributed principally to the uncertainty associated to the thickness of these nanostructures. For the majority of models used, the assumed thickness of the graphene layer is 3.4 Å, equal to the one of a graphite layer. The 3.4 Å value provides in-plane Young's modulus of the order of 1 TPa. However, several models related to graphene and single wall nanotubes have indicated thickness values ranging from 0.57 Å [17] to 6.9 Å [18]. In SWCNTs, the dispersion of mechanical properties associated with thickness and stiffness has been known as the 'Yakobson's paradox' [29]. From the modelling point of view, thickness becomes also important when considering the equivalent structural mechanics approach. Sun *et al* [30] determined a thickness for the C–C bond in SWCNTs of 1.2 Å for an equilibrium length of 1.42 Å, coupling chemical potentials with Kirchhoff–Love thin shell theory. However, the use of an isotropic thin shell can be considered valid for nanotubes with radius/thickness ratio higher than 10 [31], and for the first order of error of the ratio between atomic spacing and SWCNT radius [32]. In [33], the thickness of the Euler–Bernoulli (EB) beam element representing the C–C bond for a carbon nanotube is 1.47 Å, corresponding to an equilibrium length of 1.42 Å. On the other hand, EB theory can be applied only to slender beams with aspect ratios higher than 10 [38]. An improved model has been proposed by Scarpa and Adhikari [33] considering deep beam theory, where shear correction factors depending on the cross-section and Poisson's ratio of the equivalent C–C bond material are taken into account. Using the AMBER force model [41], the thickness value for the C–C bond for 1.42 Å of length is 0.84 Å, with a Poisson's ratio of 0.0032. The C–C bond has therefore a negligible mechanical lateral deformation when stretched or compressed, behaving like cork [26].

Reddy *et al* [23] have also highlighted the variation in bond lengths present in finite graphene sheets, as well as the in-plane orthotropy of single GS. Equilibrium bond lengths in finite graphene sheets up to 120 atoms have been observed varying between 1.39 and 1.47 Å under potential energy minimization for different in-plane loading behaviour. Special orthotropy [37] has also been recorded in two and four straight edges SGS configurations, with anisotropy degree between 0.92 and 0.99 [23]. The special orthotropy behaviour is particularly interesting, because it is also observed in common structural honeycomb configurations, even when regular hexagonal topologies are considered [27]. The other linear elastic models available for SGS predict however an isotropic in-plane mechanical behaviour, with Young's modulus Y constant along the principal directions, with in-plane shear modulus G obeying the relation $G = Y/2/(1+\nu)$. Analytical models of structural honeycombs and cellular solids are able to simulate in-plane mechanical properties [36, 37]. Structural honeycombs have ribs made of elements behaving like structural beams, with stretching and bending capabilities, and hinging important for high relative densities and damage at the base of the ribs [36].

In this work we develop closed form solutions for the in-plane elastic properties of SLGS using mechanical

cellular solids combined with equivalent atomistic-continuum mechanics approaches. A full analytical truss-lattice model of the SGS based on the geometry proposed in [18] is developed, and the rigidity matrix coefficients computed. A cellular solid micromechanics model is also developed for the hexagonal honeycomb configuration of the graphene, based on the theoretical framework proposed by Masters and Evans [36]. The evaluation of the force constants to be used in this model is based on the equivalent mechanical properties of the C–C bond. Using a deep beam theory model with Timoshenko shear correction factor, it is possible to determine the thickness, Poisson's ratio and equivalent Young's modulus of the C–C bond material, and use this values to provide the stretching, flexural and hinging capabilities of the equivalent beam elements constituting the SGS lattice. Equilibrium C–C bond lengths are evaluated from models of the braced-truss and honeycomb lattice using finite element models with 2096 atoms under different in-plane loading (uniaxial and pure shear). The models are used to identify bond lengths and thickness distributions related to minimum potential energy configurations for imposed strains up to 0.01%. The finite element results provide a benchmark of the analytical models developed, together with a critical assessment from results in open literature.

2. Braced-truss model truss-lattice model

A kinematically stable hexagonal truss-structure model can be derived analytically from the one proposed by Odegard *et al* [18], in figure 1. Elements **a**, **b**, **c**, **d**, **e** and **f** are representative of stretching effects on the C–C bonds, while the rods *g, h, i, l, m* and *n* provide the in-plane bending stiffness of the graphene layer. In a truss-like structure, the equivalent in-plane properties can be calculated from the rigidity matrix **T**, the product between the stress–strain matrix and thickness of the material [28]:

$$\mathbf{T} = \begin{bmatrix} T_{11} & T_{12} & T_{16} \\ T_{12} & T_{22} & T_{26} \\ T_{16} & T_{26} & T_{66} \end{bmatrix} \quad (1)$$

where the rigidity matrix coefficients T_{ij} are defined as:

$$T_{11} = \sum_{i=1}^{6} r_i \cos^4 \alpha_i \quad (2a)$$

$$T_{12} = \sum_{i=1}^{6} r_i \cos^2 \alpha_i \sin^2 \alpha_i \quad (2b)$$

$$T_{16} = \sum_{i=1}^{6} r_i \cos^3 \alpha_i \sin \alpha_i \quad (2c)$$

$$T_{22} = \sum_{i=1}^{6} r_i \sin^4 \alpha_i \quad (2d)$$

$$T_{26} = \sum_{i=1}^{6} r_i \cos \alpha_i \sin^3 \alpha_i \quad (2e)$$

$$T_{66} = \sum_{i=1}^{6} r_i \cos^2 \alpha_i \sin^2 \alpha_i. \quad (2f)$$
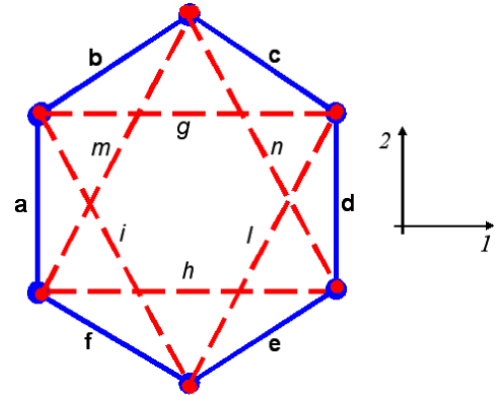

Figure 1. Unit cell for braced-truss model.

In ((2*a*)–(2*f*)), α_i are the rod angles versus the reference frame **12**. The rigidity matrix coefficients are expressed in terms of bar forces $r_i = A_i Y_i / b_i$ and the bar row spacings $b_i = \Delta A / l_i$, where $\Delta A = 3\sqrt{3} L^2 / 2$ is the area of the hexagonal unit cell. The equivalent Young's moduli for the rods **a–f** and *g–n* are computed starting from Odegard approach [18]:

$$Y_{\mathbf{a}-\mathbf{f}} = \frac{4 L k_r}{\pi d_s^2} \quad (3)$$

$$Y_{g-n} = \frac{16 k_\theta}{\pi L d_b^2} \quad (4)$$

where k_r and k_θ are stretching and rotational force constants, and the suffix s and b stands for the stretching rods **a–f** and bending rods *g–n*. The rods are assumed to have a circular cross-section. Applying (4) and (5) into the bar forces, bar spacing and coefficient definitions (2), one obtains the rigidity matrix:

$$\mathbf{T} = \left\{ \frac{\sqrt{3}}{L^2} \left(k_r L^2 + 36 k_\theta \right) \right\} \begin{bmatrix} 1 & 1/3 & 0 \\ 1/3 & 1 & 0 \\ 0 & 0 & 1/3 \end{bmatrix}. \quad (5)$$

Considering the graphene layer under in-plane stress, the uniaxial Young's moduli E and is:

$$E = \frac{1}{d_{\max}} \frac{4\sqrt{3}}{9 L^2} \left(k_r L^2 + 12 k_\theta \right) \quad (6)$$

where $d_{\max}$ is the maximum thickness between d_s and d_b. The in-plane shear modulus G_{12} is given by:

$$G_{12} = \frac{1}{d_{\max}} \frac{4\sqrt{3}}{27 L^2} \left(k_r L^2 + 12 k_\theta \right). \quad (7)$$

The coupling uniaxial–shear terms T_{i6}, with $i = 1, 2$ are zero, while $T_{11} = T_{22}$. The kinematically stable hexagonal truss is isotropic, with shear modulus always given by T_{12}. The Poisson's ratio ν for the graphene layer, in this model, is equal to 1/3. This value of Poisson's ratio is common for all equivalent continuum mechanical properties of single layer truss structures [28]. It is worth noticing that the rigidity matrix coefficients are not function of the thickness d_s and d_b—the model would lead the same results if a single constant thickness is assumed both for the stretching and bending elements.

3

3. Continuum beam for C–C bond

A common approach to describe the total steric potential energy of the C–C bonds in a CNT or graphene sheet under small linear elastic deformations is the harmonic representation, omitting the electrostatic interaction [19]:

$$U_{\text{total}} = U_r + U_\theta + U_\tau \qquad (8)$$

where U_r, U_θ and U_τ are respectively the energies due to bond stretching, bond angle variation, and combined dihedral angle and out-of-plane torsion. Following, the single terms in (8) can be expressed as [19, 33]:

$$U_r = \tfrac{1}{2}k_r \, (\Delta r)^2 \qquad (8a)$$

$$U_\theta = \tfrac{1}{2}k_\theta \, (\Delta \theta)^2 \qquad (8b)$$

$$U_\tau = \tfrac{1}{2}k_\tau \, (\Delta \varphi)^2 \qquad (8c)$$

where k_r, k_θ and k_τ are respectively the force constants related to bond stretching, bending and torsional stiffness. Bond stretching variation, in-plane and twisting angle increments are indicated by Δr, $\Delta \theta$ and $\Delta \varphi$ respectively. In the equivalent structural network approach, the elastic constants for the equivalent continuum material composing the C–C bonds are determined equating the interatomic interaction energies and the strain energies associated to the mechanical deformation of the structural elements. Assuming that the C–C bonds behave as uniform three-dimensional beams with stretching, torsion and bending capabilities, the strain energies associated to pure axial and torsion loading can be expressed as [33]:

$$U_{\text{axial}} = \frac{1}{2} K_{\text{axial}}(\Delta L)^2 = \frac{EA}{2L}(\Delta L)^2 \qquad (9a)$$

$$U_{\text{torsion}} = \frac{1}{2} K_{\text{torsion}}(\Delta \beta)^2 = \frac{GJ}{2L}(\Delta \beta) \qquad (9b)$$

$$U_{\text{bending}} = \frac{1}{2} K_{\text{bending}}(2\alpha)^2 = \frac{EI}{2L}\frac{4 + \Phi}{1 + \Phi}(2\alpha)^2. \qquad (9c)$$

In (9a) and (9b), E and G are the equivalent Young's and shear moduli for the bond, while A and J are the cross-section area and polar moment of inertia. The axial deformation and end beam rotation are expressed by ΔL and $\Delta \beta$. Equation (9c) is related to a deep uniform beam with cross-section shear deformation, second moment of area I under pure bending, with 2α being the change in rotational angle (bond angle variation [33]). The shear deformation constant Φ is defined as [38]:

$$\Phi = \frac{12EI}{GA_{\text{s}}L^2} \qquad (10)$$

where $A_{\text{s}} = A/F_{\text{s}}$, and F_{s} is the shear correction factor. Considering the C–C bond as a prismatic beam with circular section, the area and inertia properties of the beam are $A = \pi d^2/4$, $I = \pi d^4/64$ and $J = \pi d^4/32$, where d is the diameter (thickness) of the bond. The optimum shear deflection constant for circular cross-section is provided by Timoshenko's formula [39]:

$$F_{\text{s}} = \frac{6 + 12\nu + 6\nu^2}{7 + 12\nu + 4\nu^2} \qquad (11)$$

where ν is the Poisson's ratio of the beam element material. Imposing the equivalence between Δr and ΔL, as well as between $\Delta \beta$ and $\Delta \theta$, one can obtain the following expressions for the Young's and shear modulus from the equivalence between the steric and mechanical strain energies:

$$E = \frac{4k_r L}{\pi d^2}, \qquad (12a)$$

$$G = \frac{32k_\tau L}{\pi d^4}. \qquad (12b)$$

If one assumes that the equivalent material for the C–C beam is isotropic, the condition $\nu = -1 + (E/2/G)$ with $-1 < \nu < 0.5$ leads to the following maximum condition for the thickness value:

$$d < 2\sqrt{6}\sqrt{\frac{k_\tau}{k_r}}. \qquad (13)$$

From (13), using the Morse force model [40] and the torsion constant from [42] ($k_r = 84.7$ nN Å^{-1}, $k_\tau = 2.78$ nN Å rad^{-2}), the limiting value for the thickness would 0.887 Å. With a AMBER force field used for the bond [41, 33] ($k_r = 65.2$ nN Å^{-1}, $k_\tau = 2.78$ nN Å rad^{-2}), the limit value would 1.01 Å. Substituting (11) in (10) with the moduli definitions (12), the shear correction factor becomes:

$$\Phi = \frac{3k_r d^4 \left(6 + 12\nu + 6\nu^2\right)}{32k_\tau L^2 \left(7 + 12\nu + 4\nu^2\right)}. \qquad (14)$$

Inserting (14) and (12a) in (9c), and equating the bending strain energy with the angle deformation one from (8c), one obtains the following relation:

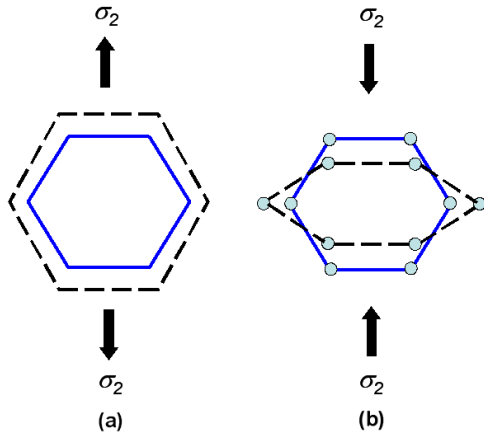$$k_\theta = \frac{k_r d^2}{16}\frac{4A + B}{A + B} \qquad (15)$$

where:

$$A = 112L^2 k_\tau + 192L^2 k_\tau \nu + 64L^2 k_\tau \nu^2 \qquad (16a)$$

$$B = 9k_r d^4 + 18k_r d^4 \nu + 9k_r d^4 \nu^2. \qquad (16b)$$

Equation (15) can be solved for d and ν for a fixed L using a nonlinear optimization approach like a Marquardt algorithm.

4. Equivalent honeycomb graphene model

An equivalent honeycomb graphene (EHG) model can be derived from Masters and Evans approach [36] used to predict the mechanical properties of cellular solids. The C–C bonds are treated like structural elements having hinging, stretching, bending and shear beam deformation capabilities. For each type of deformation, a particular force constant $K = F/\delta$ is identified, where F is the force associated to the mechanical loading, and δ the corresponding equivalent displacement. For the stretching deformation, the force constant is provided by the stretching parameter k_r. Hinging at the base of the

Figure 2. Equivalent hexagonal honeycomb cell under (a) stretching, (b) hinging.

Figure 3. C–C bond undergoing hinging for (a) compressive and (b) tensile loading along direction 2.

honeycomb rib is associated to the shear modulus of the core material, with a related force constant [36]:

$$K_h = \frac{GA}{L} \qquad (17)$$

where G is the shear modulus of the equivalent core material. Inserting (12b) in (17), the hinging spring constant is therefore:

$$K_h = \frac{8k_\tau}{d^2}. \qquad (18)$$

The bending force constant is associated to the Euler–Bernoulli beam deflection mechanism [38], with the spring constant equal to:

$$K_b = \frac{F}{L\Delta\theta} \qquad (19)$$

where $\Delta\theta = FLd/2EI$. Considering the expression (12a) for the equivalent Young's modulus of the C–C bond, the bending force constant becomes:

$$K_b = \frac{k_r}{8} \frac{d}{L}. \qquad (20)$$

The force constant K_s associated with the shear beam deflection is given by [38]:
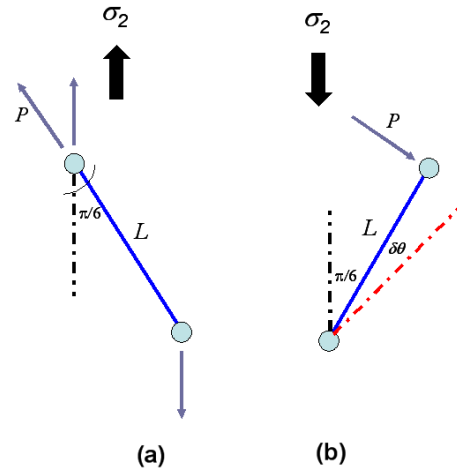
$$K_s = \frac{12EI}{L^3} \frac{1}{1+\Phi}. \qquad (21)$$

Inserting (14) and (12) in (21), the value of K_s is:

$$K_s = \left\{ 12k_r k_\tau d^2 (7 + 12\nu + 4\nu^2) \right\} \left\{ 112L^2 k_\tau + 192L^2 k_\tau \nu \right.$$
$$\left. + 64L^2 k_\tau \nu^2 + 9k_r d^4 + 18k_r d^4 \nu + 9k_r d^4 \nu^2 \right\}^{-1}. \qquad (22)$$

4.1. Stretching and hinging deformation

Figure 2 shows the overall deformation behaviour of a graphene layer unit cell subjected to pure stretching (a) and pure hinging (b). When adapting the Masters and Evans model [36] to the SLGS, both the horizontal and oblique ribs of the honeycomb have length L, while the internal cell angle θ is fixed at 30°. Considering only the stretching and hinging

contributions (figure 3), the equations for the in-plane Young's modulus E_1 can be derived as:

$$E_1 = \frac{4\sqrt{3}k_r K_h}{3d(k_r + 3K_h)}. \qquad (23)$$

The Poisson's ratio $\nu_{12} = -\varepsilon_2/\varepsilon_1$ obtained by loading along the 1-direction is recast as:

$$\nu_{12} = \frac{1 - K_h/k_r}{1 + 3K_h/k_r}. \qquad (24)$$

When considering loading along direction 2, one can identify in a similar manner the Young's modulus E_2 and the Poisson's ratio ν_{21} [36]:

$$E_2 = \frac{4\sqrt{3}k_r K_h}{3d(k_r + 3K_h)} \qquad (25)$$

$$\nu_{21} = \nu_{12} = \frac{1 - K_h/k_r}{1 + 3K_h/k_r}. \qquad (26)$$

Considering a plane stress deformation field for the SLGS, the coefficients of the rigidity matrix are:

$$T_{11} = T_{22} = \frac{\sqrt{3}k_s(k_r + 3K_h)}{6(k_r + K_h)} \qquad (27)$$

$$T_{12} = T_{21} = \frac{\sqrt{3}k_s(1 - K_h/k_r)}{6(1 + K_h/k_r)}. \qquad (28)$$

For the in-plane shear modulus G_{12} in pure shear (figure 4(a) for the stretching effect, figure 4(b) for the hinging one), model [36] for the graphene lattice case would provide:

$$G_{12} = \frac{\sqrt{3}K_h k_r}{3d(k_r + K_h)}. \qquad (29)$$

The rigidity matrix coefficient T_{66} would be therefore:

$$T_{66} = \frac{\sqrt{3}K_h k_r}{3(k_r + K_h)}. \qquad (30)$$

It is possible to notice how the GS in-plane properties under stretching–hinging deformation only are isotropic, with $G_{12} = E_1/2/(1 + \nu_{12})$.
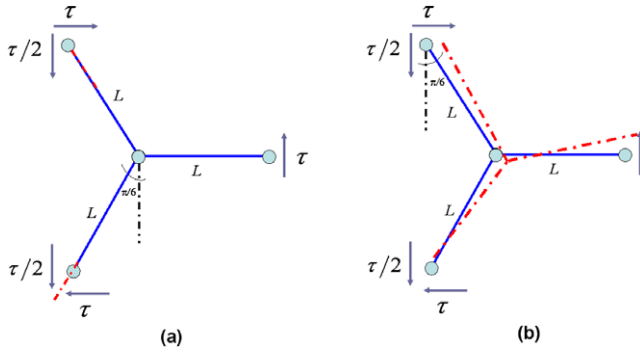
Figure 4. (a) Unit cell under shearing forces; (b) deformation due to shearing.

4.2. Bending and shear beam deformation

The strain along direction 1 caused by equivalent bending of the bond can be defined using the bending force constant K_b as [36]:

$$^b\varepsilon_1 = \frac{\sigma_1 d\sqrt{3}}{4K_b} \qquad (31)$$

where σ_1 is the applied in-plane stress along the direction 1. In structural honeycombs, the deformation provided by deep beam bending is taken into account as separate contribution to the overall mechanical properties [37]. The strain along the 1-direction is therefore similar to equation (31):

$$^\theta\varepsilon_1 = \frac{\sigma_1 d\sqrt{3}}{4K_s}. \qquad (32)$$

Considering the total strain given by all the deformation mechanisms, the Young's modulus E_1 can be derived as [36]

$$E_1 = \frac{\sigma_1}{\varepsilon_1}$$
$$= \frac{4\sqrt{3}K_b K_h k_r K_s}{3d\,(k_r K_s K_h + K_b K_h k_r + K_b K_s k_r + 3K_b K_h K_s)}. \qquad (33)$$

In a similar way, the strains along direction 2 arising from bending are:

$$^b\varepsilon_2 = \frac{\sigma_1 d\sqrt{3}}{4K_b}. \qquad (34)$$

A similar expression to (34) can be obtained for the induced strain caused by the shear beam deflection, substituting K_b with K_s. The bending terms provide a deformation opposing the one given by the stretching mechanism. Applying the definition of Poisson's ratio ν_{12} one would obtain [36]:

$$\nu_{12} = -\frac{\varepsilon_2}{\varepsilon_1} = \frac{M-N}{M+3N} \qquad (35)$$

where:

$$M = K_s k_r K_h + K_b K_h k_r + K_b K_s k_r \qquad (36a)$$

$$N = K_b K_s K_h. \qquad (36b)$$

For the uniaxial properties along direction 2, using a similar approach one can obtain [36]:

$$E_2 = \frac{4\sqrt{3}K_b K_h k_r K_s}{3d\,(k_r K_s K_h + K_b K_h k_r + K_b K_s k_r + 3K_b K_h K_s)} \qquad (37)$$

$$\nu_{21} = -\frac{\varepsilon_1}{\varepsilon_2} = \frac{M-N}{M+3N}. \qquad (38)$$

The equivalent shear modulus G_{12} from the Masters and Evans adaptation to the SLGS case would be:

$$G_{12} = \frac{\sqrt{3}K_b K_h k_r K_s}{3d\,(k_r K_s K_h + K_b K_h k_r + K_b K_s k_r + K_b K_h K_s)}. \qquad (39)$$

Also in this case, one can observe the isotropic in-plane properties of an infinite SLGS by the satisfaction of the condition $G_{12} = E_1/2/(1 + \nu_{12})$.

5. Numerical models

Finite size graphene sheet finite element models were assembled using a technique similar to [19]. Each rod of the braced-truss unit cell was represented by a single uniaxial element with tension–compression capabilities, linear interpolation functions and translation degrees of freedom along the 1 and 2 directions. The node at the junction of each uniaxial element corresponds to a single atom in the graphene lattice, with overall 2096 atoms for the whole model (length 79.93 Å, width 68.87 Å). The uniaxial loading conditions were represented by uniform displacements at the end of the graphene sheet corresponding to an imposed strain of 0.01%, while the opposite end of the sheet had the degrees of freedom corresponding to the loading direction blocked to represent a sliding condition (figure 5(a)). The in-plane Poisson's ratio was calculated averaging the side normal displacements and calculating the corresponding strains [43]. For the pure shear loading, a uniform shear strain γ was imposed on the edges of the sheet, and the in-plane shear modulus calculated from the estimation of the strain energy U of the system [38]. The nodes at the edge were loaded with imposed horizontal and vertical displacements u and v, to represent the strain $\gamma = \partial u/\partial y + \partial v/\partial x$ [18]. For each type of loading, the average equilibrium C–C bond length L and thickness d_s and d_b were identified using a multistep optimization route, involving the minimization of the total strain energy of the system using zero order and first order derivative techniques [44].

The honeycomb lattice finite element models (figure 5(b)) were developed following a similar approach. The C–C bonds were simulated using 2-nodes beam elements having axial bending and shear deformation capabilities in 3D with six degrees of freedom (three translations and three rotations). Similarly to the braced-truss models, loading was performed along the 1 and 2 directions, and pure shear was imposed on the edges of the sheet. The minimization of the potential energy was carried out during the different loading conditions to identify the equilibrium length of the C–C bond, as well as the thickness d and the bond Poisson's ratio ν. An added constraint relation imposing the isotropic condition for the equivalent C–C bond material was inserted in the optimization set of equations.
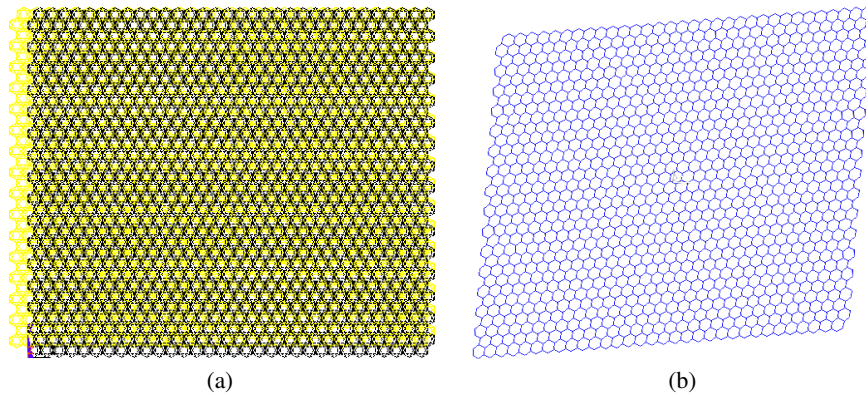
Figure 5. (a) Finite element of braced-truss single layer graphene sheet under tensile loading along *x*-direction; (b) finite element of honeycomb single layer graphene sheet under pure shear loading.

Table 1. In-plane rigidity for braced-truss graphene model.

Force field	E (TPa) (equation (6))	G_{12} (TPa) (equation (7))	ν_{12}	E_1 (TPa) (FE)	E_2 (TPa) (FE)	G_{12} (TPa) (FE)	ν_{12} (FE)	ν_{21} (FE)
AMBER	1.222	0.143	0.33	1.303	1.378	0.208	0.569	0.567
Morse	1.910	0.181	0.33	1.957	1.379	0.213	0.570	0.578

6. Results and conclusions

6.1. Braced-truss model

For the braced-truss model, the AMBER force constants used were $k_r = 32.6$ nN Å^{-1} and $k_\theta = 0.438$ nN Å rad^{-2} [18, 19]. A modified version of the linearized Morse potential [40] ($k_r = 42.3$ nN Å^{-1} and $k_\theta = 0.45$ nN Å rad^{-2}) was adopted to accommodate the total mechanical strain energy of the truss as indicated by Odegard *et al* [18]. The C–C lengths and thickness of the rods used in the analytical calculations have been the ones determined through the finite element minimization technique. For the AMBER case, the loading along direction 1 leads to the equilibrium C–C bond length of 1.39 Å, while for the case of mechanical loading along 2 the same length is 1.35 Å, also for the pure shear case. The Morse case provides a C–C length for loading along direction 1 of 1.45 Å, while for the case on direction 2 the length is 1.35 Å, and for pure shear 1.36 Å. The thickness distribution provides very different values for the rods **a**–**f** and struts *g*–*n*. For loading along direction 1, rods **a**–**f** have thickness $d_s = 0.565$ Å, regardless of the force model used. The same is valid also for loading along direction 2 and pure shear, with a thickness value 0.55 Å. Rods *g*–*n* thickness have a different behaviour. For the AMBER case with loading along 1 axis, the thickness d_b is 2.24 Å, while for the Morse force model the same thickness is 1.81 Å. For loading along direction 2, the two force models provide a thickness of 2.22 Å, while for pure shear both AMBER and Morse potentials give a d_b value of 6.4 Å. All these thickness values are lower than the 6.9 Å indicated in [18], although in the same reference the maximum thickness for the braced unit cell under pure shear is reported as 5.7 Å.

The analytical expressions for the Young's and shear modulus (6) and (7) provide a conservative estimation compared to the values from the finite element simulations (table 1). The variation in Young's modulus between the AMBER analytical and FE results is around 10%, while a more significant discrepancy is recorded for the shear modulus (32%). The degree of anisotropy (E_1/E_2) 0.94 is in line with the one observed in finite size graphene sheet [23]. On the other hand, the Morse linearized potential provides a far greater anisotropy degree (0.71). All force models provide in-plane Poisson's ratio around 0.56, higher than the analytical 0.33, as well as the 0.44 reported in [19].

6.2. Bond thickness and length

The minimization of equation (15) leads to different results according to the force model used. With the AMBER force constants, the thickness of the C–C bond would be 0.84 Å, with a Poisson's ratio ν of 0.034 for an equilibrium length L of 1.38 Å. For the linearized Morse potential, the thickness is decreased to 0.74 Å, while the Poisson's ratio is 0.043, for the same equilibrium length of 1.38 Å. The thickness results are compatible with different results in open literature, such as the ones of Zhou *et al* [46] ($d = 0.74$ Å), Tu and Ou-Yang [45] ($d = 0.75$ Å) and Pantano *et al* [51] ($d = 0.75$ Å). The results from the linearized Morse potential are closer to the values provided by Kudin *et al* [13] ($d = 0.87$ Å) and Goupalov [52] ($d = 0.85$ Å). Moreover, the thickness and equivalent Poisson's ratio calculated using the AMBER force field are the same to the ones calculated by Scarpa and Sondipon in [35]. For both Poisson's ratio values, the C–C bond features a negligible transverse dilation when mechanically stretched. The equilibrium length of the C–C bond is different from the one of 1.42 Å used in [35], but within the range of sizes available in open literature. Reddy *et al* [23] have recorded length distributions in finite size graphene sheets between 1.39 Å (at the middle of the GS), to 1.47 Å (near

Table 2. Force constants for equivalent honeycomb model.

Force field	K_r (nN Å^{-1})	K_h (nN Å^{-1})	K_b (nN Å^{-1})	K_s (nN Å^{-1})
AMBER	65.2	31.5	4.96	12.1
Morse	84.7	40.6	5.67	13.1

the corners). Duplock *et al* [1] report ranges of C–C bond lengths between 1.37 and 1.54 Å when Stone–Wales defects are present.

6.3. Equivalent honeycomb model

Table 2 shows the force constants for the stretching, hinging, beam shear and flexural bending for the EH model according to the two atomic potentials used. The values of the C–C lengths L, thickness d and Poisson's ratio ν are obtained from the minimization of equation (15). For all cases, the flexural bending stiffness constant K_b provides the lowest value between the different deformation mechanisms. Therefore, an equivalent structural honeycomb model for the grapheme sheet including all the stiffness terms would have a deformation dominated by the in-plane bending of the bonds. The AMBER force field model provides a shear beam stiffness K_s comparatively higher than the one from the linearized Morse potential, when considered against the hinging stiffness constant K_h (K_s/K_h is 0.384 for AMBER, 0.322 for Morse). The flexural stiffness ratios K_b/K_h are very similar for the two models, with values between 0.139 and 0.157. The effect of the honeycomb force constants (18), (20) and (22) over the analytical mechanical properties of the honeycomb lattice can be estimated from table 3. When only the stretching–hinging deformation mechanism is considered, the in-plane Poisson's ratio ν_{21} is between 0.211 and 0.213. The AMBER model would provide an in-plane Young's modulus around 3.5 TPa, while for the linearized Morse case there is an increased stiffness by a factor 1.47. For both cases, the isotropic in-plane material condition seems satisfied, with $G_{12} \sim E_1/2/(1 + \nu_{12})$. We notice that the value of 3.536 TPa for the AMBER model is approaching the 3.81 TPa calculated by Huang *et al* [17] using first generation TB potentials, although the latter correspond to an in-plane Poisson's ratio ν_{12} of 0.412, almost twice higher than the one provided by our model. Caillerie [25] and Chang and Gao [50] provide a closed form solution for the stretching–hinging model, with in-plane Poisson's ratios 0.26 and 0.16 respectively, in line with our predictions. The tensile rigidity Ed for the stretching–hinging model using the AMBER force field (table 5) is also similar to the ones calculated by Brenner *et al* [15] (overestimation of 21%), Huang *et al* [17] (overestimate of 18%), and Reddy *et al* [23] (overestimate of 23%), while there is a fairly good agreement with Caillerie *et al* [25], with a tensile rigidity 6.3% higher. The Morse potential provide an overall stiffening effect, providing tensile rigidities similar to the ones from Zhou *et al* [46], Tu and Ou-Yang [45], Yakobson *et al* [47], Sakhaee-Pour [34] and Kudin *et al* [13]. In those cases, the estimation errors are respectively 2%, 3%, 5.5%, 8% and 10%, although the Poisson's ratios for [45, 34] and [15] are significantly higher than the ones predicted for this model. Also, although

Table 3. In-plane rigidity for equivalent honeycomb model.

Stretching–hinging ($K_b \to \infty$, $K_s \to \infty$)				
Force field	E_1 (TPa)	E_2 (TPa)	ν_{12}	ν_{21}	G_{12} (TPa)
AMBER	3.536	3.536	0.211	0.211	1.464
Morse	5.189	5.189	0.213	0.213	2.135

Stretching–hinging-shear beam ($K_b \to \infty$)				
Force field	E_1 (TPa)	E_2 (TPa)	ν_{12}	ν_{21}	G_{12} (TPa)
AMBER	1.714	1.714	0.617	0.617	0.524
Morse	2.284	2.284	0.653	0.653	0.689

All deformation mechanisms				
Force field	E_1 (TPa)	E_2 (TPa)	ν_{12}	ν_{21}	G_{12} (TPa)
AMBER	0.762	0.762	0.830	0.830	0.202
Morse	1.000	1.000	0.848	0.848	0.270

Hemmasizadeh *et al* [24] predict a Young's modulus of 0.939 TPa in line with Rajendran *et al* [23], Sakhaee-Pour [34] and Chang and Gao [50], the tension rigidity is 60% lower, due to the thickness of 1.317 Å calculated. When considering the other deformation mechanisms, the effect is to increase the in-plane Poisson's ratio, and at the same time decrease the stiffness. When the shear beam deflection is included in the model (table 3), the Poisson's ratio increases by a factor in the range 2.9–0.617 and 0.653, for the AMBER and Morse cases, respectively. Although our model predicts higher in-plane Poisson's ratio values, it seems to indicate that a further deformation mechanism other than stretching and hinging could be considered when dealing in finite size graphene sheets [23], or using first and second generation Brenner potentials [17]. In terms of Poisson's ratios, the high values from Sakhaee-Pour [34] are closer to the full EHM models, both with the AMBER and linearized Morse potentials. There is however a considerable lowering of the in-plane rigidity, being 58% and 35% lower than the case from Reddy *et al* [23] when considering AMBER and Morse potentials respectively. The in-plane Young's modulus for the stretching–hinging shear beam case is similar in terms of order of magnitude to the one proposed by the FE braced-truss models, while the Poisson's ratio from the FE simulations compare well with the EHM model. The tension rigidities, however, are still lower than the ones provided by the braced-truss models, the latter being 0.273 TPa nm and 0.420 TPa nm for the AMBER and Morse cases respectively. The inclusion of all the deformation mechanisms leads to a more significative decrease of the in-plane stiffness and increase of the Poisson's ratio, the latter tending towards the unity. It must be noted, however, that the values of the Young's moduli (0.762 and 1.0 TPa) are in line with the ones predicted by the Cauchy–Borne rule from Reddy *et al* [23], although the latter use a thickness d of 3.4 Å for their calculations. Structural honeycombs with regular hexagonal topology have an in-plane Poissons' ratio of 1 when only bending of the ribs is considered [36, 37], while lower values have to be expected when shear deformation of the bending beams is considered [43]. Sakhaee-Pour [34] predicts in-plane Poisson's ratios varying between 1.129 and 1.441 based on the chirality of the SLGS. The special orthotropy of hexagonal

honeycombs also implies that the cross relation $E_1\nu_{21} = E_2\nu_{12}$ is valid, therefore not putting a specific limit the in-plane Poisson's ratio values [36, 37, 43].

The results from the simulations on the finite size graphene sheets via the finite element models are illustrated in table 4. When loading along direction 1, the in-plane Young's modulus E_1 varies between 4.248 and 4.712 TPa, providing values close to the 4.23 TPa from Huang *et al* cite17 using second generation TB potentials, although for the latter the in-plane Poisson's ratio is lower (0.397 against 0.517 and 0.546 from our predictions). The average C–C bond length after minimization of the potential energy during loading is 1.35 Å and 1.42 Å for the AMBER and Morse case respectively, while the thickness d (0.82 and 0.86 Å) are also different from the ones identified from the single C–C bond minimization (15). It is noteworthy to observe the equivalent Poisson's ratio ν for the C–C bond material. While for the Morse potential case the final ν tends towards the one of an elastomer (0.431), the one related to the AMBER force model is slightly auxetic [53, 54] ($\nu = -0.008$), similar to low volumetric compression ratio foams [55]. When loading along direction 2, the thickness of the ribs increase to 0.99 and 0.87 Å for the AMBER and Morse cases, with equilibrium lengths L between 1.35 and 1.36 Å. The equivalent Poisson's ratios ν for the C–C bonds are between 0.455 and 0.459. These values of ν suggests that under these loading conditions, the finite size SLGS has an equivalent hyperelastic behaviour under small deformations, in good agreement with equivalent Mooney–Rivlin models used for the large deformation of single wall carbon nanotubes [56]. The finite size of the SLGS leads to a degree of anisotropy for the in-plane properties, being equal to 0.81 for the AMBER case, 0.99 for the Morse one, apparently opposite to what is recorded for the finite size braced-truss model. The pure shear loading provides transverse shear values between 1.374 and 1.764 TPa, in line with the braced-truss model predictions. The equilibrium lengths are 1.35 Å, with thickness of the bonds of 0.55 Å, similar to the 6.4 Å recorded for the braced-truss models. The in-plane tension rigidities also correspond to the ones of Sakhaee-Pour [34] for the AMBER case (0.072–0.079 TPa nm). The equivalent ν for the C–C bond material is strongly auxetic (-0.556 and -0.419 for AMBER and Morse respectively), like for transformed open cell polyurethane foams [53]. Auxeticity in nanostructures has been recently identified in carbon nanotube paper sheets with mixed single and multiwall CNT under bending and stretching [57]. The in-plane shear modulus (1.374 and 1.764 TPa) are in line with the ones predicted by the stretching–hinging theoretical model. The tension rigidities corresponding to pure shear (0.076 and 0.097 TPa nm), compare with the ones from Reddy *et al* [23] (0.06 TPa nm for two straight edges finite size SLGS). For all cases, the identified equilibrium lengths of the C–C bonds through minimization of the potential energy are at the lower end of the interval values in open literature.

Comparison of SLGS mechanical properties from models is usually performed considering data from bulk graphite [58]. The experimental uniaxial tensile rigidity is close to the stretching–hinging model with the Morse linearized potential, although the experimental Poisson's ratio is 33% lower than the

Table 4. Mechanical properties from potential energy minimization of FE GS.

Loading along direction 1					
Force model	L (Å)	d (Å)	ν	ν_{21}	Y_1 (TPa nm)	E_1 (TPa)
AMBER	1.35	0.82	-0.008	0.523	0.517	4.248
Morse	1.42	0.86	0.431	0.577	0.546	4.712

Loading along direction 2					
Force model	L (Å)	d (Å)	ν	ν_{12}	Y_2 (TPa nm)	E_2 (TPa)
AMBER	1.35	0.99	0.455	0.509	0.342	3.433
Morse	1.36	0.87	0.459	0.551	0.408	4.678

Pure shear					
Force model	L (Å)	d (Å)	ν	ν_{12}	Y_{12} (TPa nm)	G_{12} (TPa)
AMBER	1.35	0.55	-0.556	N/A	0.076	1.374
Morse	1.35	0.55	-0.419	N/A	0.097	1.764

predicted one. The experimental shear rigidity (0.147 TPa nm) is also close to the one predicted by the Morse stretching–hinging model (0.168 TPa nm), although the experimental shear modulus (440 TPa) is approached only by the stretching–hinging-shear beam model (table 2), in particular for the AMBER force field. Direct mechanical measurements of single graphene sheets are difficult to perform. However, Frank *et al* [59] have measured the Young's modulus and spring constants of suspended graphene sheets over silicon dioxide trenches using AFM techniques. The Young's modulus measured (0.5 TPa) is half of the one for bulk graphite. Also considering an interlayer distance of 3.35 between the sheets stacks, the tension rigidity would amount to 0.167 TPa nm, a value which is substantially lower compared to all the predicted tensile rigidities from existing MD and numerical simulations. However, we observe that the models incorporating all deformation mechanisms (including bending) provide closer predictions in terms of Young's modulus (0.762 TPa for the AMBER force field case). No data regarding Poisson's ratio and shear modulus are available from these experiments.

7. Conclusions

The main novelty of the proposed approach include:

 (1) Incorporation of additional deformation mechanisms (bending and shear deformation) for the homogenized in-plane mechanical properties of single graphene sheets, apart from the classical stretching and hinging ones. These mechanisms were not included in previous works in this area.
 (2) Inclusion of optimum shear correction factors in the equivalent atomistic-continuum beam model for the C–C bond. The improved mechanical model allows identifying via nonlinear optimization a value for the thickness and equivalent Poisson's ratio of the C–C bond.

Table 5. Graphene data from literature and present work.

Author	Y_1 (TPa nm)	Y_2 (TPa nm)	ν_{12}	ν_{21}	d (Å)
Tu and Ou-Yang [45]		0.348		0.34	0.74
Zhou *et al* [46]		0.377		0.24	0.74
Yakobson *et al* [47]		0.363		0.19	0.66
Caillerie *et al* [25]		0.277		0.26	N/A
Brenner *et al* [15]		0.235		0.41	0.62
Huang *et al* [17]		0.243		0.397	0.57
Kudin *et al* [13]		0.345		0.149	0.84
Chang and Gao [50]		0.360		0.16	3.4
Cho *et al* [48]		0.386		0.195	3.35
Sakhaee-Pour [34]		0.337–0.354		1.129–1.441	3.4
Hemmasizadeh *et al* [24]		0.124		0.19	1.317
Blakslee *et al* [58]		0.342		0.16	3.35
Lee *et al* [60]		0.335		N/A	3.35
Reddy *et al* [23]	0.228	0.277	0.43	0.52	3.4
Present FE honeycomb (AMBER)	0.517	0.342	0.523	0.509	0.82–0.99
Present FE honeycomb (Morse)	0.546	0.408	0.551	0.577	0.86–0.87
Present EHM stretching–hinging (AMBER)		0.297		0.211	0.84
Present EHM stretching–hinging (Morse)		0.384		0.213	0.74
Present EHM stretching–hinging-shear (AMBER)		0.144		0.617	0.84
Present EHM stretching–hinging-shear (Morse)		0.169		0.653	0.74
Present EHM-all deformation mechanisms (AMBER)		0.064		0.830	0.84
Present EHM-all deformation mechanisms (Morse)		0.074		0.848	0.74

(3) Derivation of the overall properties of SLGS from the individual bond properties analytical braced-truss and structural honeycomb lattice models. This enables one to bypass detailed FE calculations to estimate homogenized mechanical properties, to be used as first approximation for graphene-based composites and GS natural frequencies.

The analytical models presented allow correlating the equivalent homogenized mechanical properties of single GS with the different deformation mechanisms of the C–C bonds composing the graphene lattice. From a structural mechanics point of view, the equivalent spring constants associated to the classical stretching and hinging deformation mechanisms provide the best agreement with existing models in open literature derived with other methods. However, the bending shear force constant can be considered as an equivalent deformation mechanism to account for higher Poisson's ratio values presented in other works. The models presented allow also correlating SLGS thickness and average C–C bond length distributions to the mechanical loading exerted on finite size graphene sheets, providing again general good agreement with existing values in literature. In conjunction with strain energy minimization through finite element simulations, the refined equivalent mechanical properties for the C–C bond presented in this work allow also to identify peculiar mechanical deformations of the C–C bonds in the SLGS when represented as deep beams with axial and bending capabilities. In particular, pure shear loading seems to imply an equivalent auxetic behaviour for the bonds, with significant negative Poisson's ratio values when considering an equivalent isotropic bond material.

Acknowledgment

References

[1] Duplock E J, Scheffler M and Lindan P J D 2004 *Phys. Rev. Lett.* **92** 225502

[2] Novoselov K S, Geim A K, Morozov S V, Jiang D, Katsnelson M I, Grigorieva I V, Dubonos S V and Firsov A A 2005 *Nature* **498** 197

[3] Ohta T, Bostwick A, Seyller T, Horn K and Rotenberg E 2006 *Science* **313** 951

[4] Stankovich S, Dikin D A, Dommett G H B, Kohlhaas K M, Zimney E J, Stach E A, Piner R D, Nguyen S T and Ruoff R S 2006 *Nature* **442** 282

[5] Sakhaee-Pour A, Ahmadian M T and Vafai A 2008 *Solid State Commun.* **147** 336

[6] Dubay O and Kresse G 2003 *Phys. Rev.* B **67** 035401

[7] Kitipornchai S, He X Q and Liew K M 2005 *Phys. Rev.* B **72** 075443

[8] Couturier G, Aimé J P, Salardenne J, Boisgard R, Gourdon A and Gauthier S 2001 *Appl. Phys.* A **72** 47

[9] Zhang Y, Tan Y-W, Stormer H L and Kim P 2005 *Nature* **438** 201

[10] Sakhaee-Pour A, Ahmadian M T and Naghdabadi R 2008 *Nanotechnology* **19** 085702

[11] Bacon D J and Nicholson A J 1977 *J. Phys. C: Solid State Phys.* **10** 2295

[12] Gillis P P 1984 *Carbon* **22** 387
[13] Kudin K N, Scuseria G E and Yakobson B I 2001 *Phys. Rev.* B **64** 235406
[14] Lier G V, Alsenoy C V, Doren V V and Greelings P 2000 *Chem. Phys. Lett.* **326** 181
[15] Brenner D W 1990 *Phys. Rev.* B **42** 9458
[16] Brenner D W, Shenderova O A, Harrison J A, Stuart S J, Ni B and Sinnott S B 2002 *J. Phys.: Condens. Matter* **14** 783
[17] Huang Y, Wu J and Hwang K C 2006 *Phys. Rev.* B **74** 245413
[18] Odegard G M, Gates T S, Nicholson L M and Wise K E 2002 *Compos. Sci. Technol.* **62** 1869
[19] Li C and Chou T W 2003 *Int. J. Solids Struct.* **40** 2487
[20] Meo M and Rossi M 2006 *Compos. Sci. Technol.* **66** 1597
[21] Reddy C D, Rajendran S and Liew K M 2005 *Int. J. Nanosci.* **4** 631
[22] Rajendran S and Reddy C D 2006 *J. Comput. Theor. Nanosci.* **3** 1
[23] Reddy C D, Rajendran S and Liew K M 2006 *Nanotechnology* **17** 864
[24] Hemmasizadeh A, Mahzoon M, Hadi E and Kandan R 2008 *Thin Solid Films* **416** 7636
[25] Caillerie D, Mourat A and Raoult A 2006 *J. Elast.* **84** 33
[26] Gibson L J, Easterling K E and Ashby M F 1981 *Proc. R. Soc.* A **377** 99
[27] Bitzer T 1997 *Honeycomb Technology: Materials, Design, Manufacturing, Applications and Testing* (Berlin: Springer)
[28] Kollár L and Hegedús I 1985 *Analysis and Design of Space Frames by the Continuum Method. Developments in Civil Engineering* (Amsterdam: Elsevier) p 10
[29] Shenderova O A, Zhirnov V V and Brenner D W 2002 *Crit. Rev. Solid State Mater. Sci.* **27** 227
[30] Sun C Q, Bai H L, Tay B K, Li S and Jiang E Y 2003 *J. Phys. Chem.* B **107** 7544
[31] Timoshenko S 1940 *Theory of Plates and Shells* (New York: McGraw-Hill)
[32] Peng J, Wu J, Hwang K C, Song J and Huang Y 2008 *J. Mech. Phys. Solids* **56** 2213
[33] Tserpes K I and Papanikos P 2005 *Composites* B **36** 468
[34] Sakhaee-Pour A 2008 *Solid State Commun.* **139** 91
[35] Scarpa F and Adhikari S 2008 *J. Phys. D: Appl. Phys.* **41** 085306
[36] Masters I G and Evans K E 1996 *Compos. Struct.* **35** 403
[37] Gibson L J and Ashby M F 1997 *Cellular Solids: Structure and Property* 2nd edn (Cambridge: Cambridge University Press)
[38] Przemieniecki J S 1968 *Theory of Matrix Structural Analysis* (New York: McGraw-Hill)
[39] Kaneko T 1975 *J. Phys. D: Appl. Phys.* **8** 1927
[40] Belytschko T, Xiao S P, Schatz G C and Ruoff R S 2002 *Phys. Rev.* B 2 **65** 1
[41] Cornell W D *et al* 1995 *J. Am. Chem. Soc.* **117** 5179
[42] Jorgensen W L and Severance D L 1990 *J. Chem. Am. Soc.* **112** 4768
[43] Scarpa F, Panayiotou P and Tomlinson G 2000 *J. Strain Anal. Eng.* **35** 383
[44] Denn M M 1969 *Optimization by Variational Methods* (New York: McGraw-Hill)
[45] Tu Z and Ou-Yang Z 2002 *Phys. Rev.* B **65** 233407–10
[46] Zhou X, Zhou J and Ou-Yang Z 2000 *Phys. Rev.* B **62** 13692–6
[47] Yakobson B I, Brabec C J and Bernholc J 1996 *Phys. Rev. Lett.* **76** 2511–25
[48] Cho J, Luo J J and Daniel I M 2007 *Comput. Sci. Technol.* **67** 2399
[49] Després J F, Daguerre E and Lafdi K 2002 *Carbon* **40** 445
[50] Chang T and Gao H 2003 *J. Mech. Phys. Solids* **51** 1059
[51] Pantano A, Parks D M and Boyce M C 2004 *J. Mech. Phys. Solids* **52** 789
[52] Goupalov S V 2005 *Phys. Rev.* B **71** 085420
[53] Lakes R 1987 *Science* **235** 1038
[54] Evans K E, Nkansah M A, Hutchinson I J and Rogers S C 1991 *Nature* **353** 124
[55] Scarpa F, Ciffo L G and Yates J R 2004 *Smart Mater. Struct.* **13** 49
[56] Suzuki K and Nomura S 2007 *J. Comput. Mater.* **41** 1123
[57] Hall L J, Coluci V R, Galvão D S, Kozlov M E, Zhang M, Dantas S O and Baughman R H 2008 *Science* **320** 504
[58] Blakslee O L, Proctor D G, Seldin E J, Spence G B and Weng T 1970 *J. Appl. Phys.* **41** 3373
[59] Frank I W, Tanenbaum D M, Van der Zande A M and McEuen P L 2007 *J. Vac. Sci. Technol.* B **25** 2558
[60] Lee C, Wei X, Kysar J W and Hone J 2008 *Science* **321** 385